http://dx.doi.org/10.5012/bkcs.2012.33.12.4063

Influence of Nanoporous Oxide Substrate on the Performance of Photoelectrode in Semiconductor-Sensitized Solar Cells

Jin Ho Bang

Department of Chemistry and Applied Chemistry, Hanyang University, Kyeonggi-do 426-791, Korea
E-mail: jbang@hanyang.ac.kr
Received July 28, 2012, Accepted September 22, 2012

Oxide substrates in semiconductor-sensitized solar cells (SSSCs) have a great impact on their performance. TiO_2 has long been utilized as an oxide substrate, and other alternatives such as ZnO and SnO_2 have also been explored due to their superior physical properties over TiO_2. In the development of high-performance SSSCs, it is of significant importance to understand the effect of oxides on the electron injection and charge recombination as these two are major factors in dictating solar cell performance. In addition, elucidating the relationship between these two critical processes and solar cell performance in each oxide is critical in building up the basic foundation of SSSCs. In this study, ultrafast pump-probe laser spectroscopy and open-circuit decay analysis were conducted to examine the characteristics of three representative oxides (TiO_2, ZnO, and SnO_2) in terms of electron injection kinetics and charge recombination, and the implication of results is discussed.

Key Words : Semiconductor-sensitized solar cells, Photoelectrode, Oxide substrates, Electron injection, Charge recombination

Introduction

Semiconductor-sensitized solar cells (SSSCs) have attracted enormous interest over decades as an analogue of dye-sensitized solar cells (DSSCs) because of several superior physical properties of inorganic semiconductors over dyes, such as bandgap tunability through size quantization, high absorption coefficient (*i.e.*, extinction coefficient), better long-term stability, and multiple exciton generation (MEG) for high efficiency.[1-3] While the energy conversion efficiency of SSSCs has reached over 5% recently, it still lags behind its competitor, DSSCs, thus requiring further improvement.[4] The development of nanoporous oxide films for photoelectrode has been a mainstream of the efforts to boost up the efficiency of SSSCs. In general, a photoelectrode in SSSCs is composed of large bandgap metal oxide film sensitized with semiconductor nanoparticles (*e.g.*, CdS, CdSe, PbS, *etc*.), which possess a bandgap narrow enough to harvest visible light.[5-8] A variety of oxides have been assessed to figure out their feasibility for photoelectrode to date, but SSSCs have typically relied on nanoporous TiO_2 thin film to obtain high performance. Despite its popularity as an oxide substrate in SSSCs, several adverse physical properties of TiO_2, such as low electron mobility and short diffusion length, impose constraint on further improvement of SSSCs.[9,10] In this respect, alternative oxide materials, particularly ZnO and SnO_2, have been explored to overcome the limitation of TiO_2 as they possess superior ability in electron transport.[11,12] A number of trials to utilize ZnO and SnO_2 in SSSCs, however, have ended fruitless so far.[13,14]

The low efficiency of SSSCs in comparison to DSSCs is attributed to various factors, among which interfacial electron injection at photoelectrode and charge recombination at the interface between photoelectrode and electrolyte dominantly dictate the overall performance of solar cells.[1] These two critical processes occurred during solar cell operation are greatly influenced by inherent physical properties of oxide substrates. Therefore, understanding the effect of oxides on the electron injection and charge recombination and elucidating the relationship between these processes and solar cell performance in each oxide are of great importance in the development of high-performance SSSCs.[15] While systematic investigation on this study for DSSCs has been performed,[11,16,17] little study has been reported for SSSCs. In this study, the characteristics of CdS-sensitized oxide photoelectrodes were investigated, especially focusing on three representative oxide substrates –TiO_2, ZnO, and SnO_2– to provide insight into the nature of interfacial electron injection and charge recombination.

Experimental Section

Synthesis of CdS Quantum Dots (QDs). CdS QDs were prepared as previously reported with some modification.[18] CdO (0.4 mmol) was dissolved in 1-octadecene (17.8 mL) containing oleic acid (11 mL) by heating the mixture up to ~300 °C under inert atmosphere. Once the solution became clear and was stabilized at 300 °C, sulfur (0.28 mmol) dissolved in 1-octadecene (10 mL) was injected into the solution, and the reaction was kept at 250 °C for 10 mins to grow nanoparticles. After the reaction, the QD solution was cooled to room temperature, washed with excess acetone, and centrifuged to separate CdS QDs. The resulting QD precipitate was redissolved in toluene, washed with excess acetone and methanol three times, and finally stored in toluene for use.

Preparation of CdS QD Decorated Metal Oxide Films. Semi-transparent, thin oxide films for laser spectroscopy were prepared by spin-coating a suspension containing nano-sized oxide powder onto optically transparent electrodes (OTEs). Each oxide suspension consists of oxide nanopowder (0.3 g) in 10 g of mixed solvents (ethanol:methanol:3-ethoxy-1-propanol:*N,N*-dimethylformamide = 3:4:2:1 by weight%). Each oxide film was annealed under air at 450 °C for 30 min. The annealed film was dipped into a N_2-saturated acetonitrile solution containing 3-mercaptopropionic acid (1 M) for 24 h, washed with acetonitrile and toluene, and subsequently placed into the N_2-saturated QD solution for 48 h to sensitize oxides with CdS QDs. Thicker oxide films for photoelectrochemical measurements were fabricated using a spray deposition method where a colloidal oxide suspension was diluted with water and sprayed onto hot OTEs. The thickness of each oxide film was ~4 μm (Figure S1 in Supporting Information). Upon being cooled, the films were annealed under air at 450 °C for 30 min, and the same procedures described above were repeated to anchor CdS QDs onto each oxide film.

Characterization. UV-vis absorption and photoluminescence spectra of CdS QDs were recorded using a Varian CARY50 Bio UV-visible spectrophotometer and Jobin Yvon Horiba FluoroMax-3 spectrofluorometer, respectively. Oxide films were analyzed with an X-ray diffractometer (Scintag X1 advanced diffraction system) and a field-emission scanning electron microscope (Hitachi S-4500 FESEM). Ultrafast transient absorption spectroscopy was carried out using a Clark-MXR 2010 Ti:Sapphire laser system (775 nm, 1 mJ/pulse, full width at half-maximum of 130 fs, and 1 kHz repetition rate) equipped with a CCD spectrograph (Ocean Optics, S2000-U-UV-vis). 5% of the fundamental was used to generate a probe pulse, while 95% of the laser beam was utilized by a second harmonic generator to produce a laser pulse for pump (387 nm). Before laser excitation, all thin film samples were thoroughly degassed to avoid possible degradation of CdS QDs during the measurement.

Photoelectrochemical Measurements. Photocurrent and photovoltage measurement were performed using a two-armed cell with Au-gauze counter electrode in N_2-saturated, aqueous 0.1 M Na_2S solution as a redox couple. Data were collected using a Keithley 2601 sourcemeter under the illumination of collimated, filtered light ($\lambda > 300$ nm, 100 mW/cm^2) from an Oriel 450 W xenon arc lamp. Prior to the measurement, N_2 gas was purged through the electrolyte for 30 mins to ensure oxygen-free atmosphere.

Results and Discussion

Electron Injection Kinetics. Differences in electron injection kinetics were explored using three oxide films (TiO_2, ZnO, and SnO_2) sensitized with CdS QDs as a model system. CdS QDs were prepared using a conventional hot injection method. The prepared CdS QDs exhibited typical absorption characteristic with a first excitonic peak at ~475 nm and a band-edge emission centered at 480 nm (Figure 1(a)). CdS

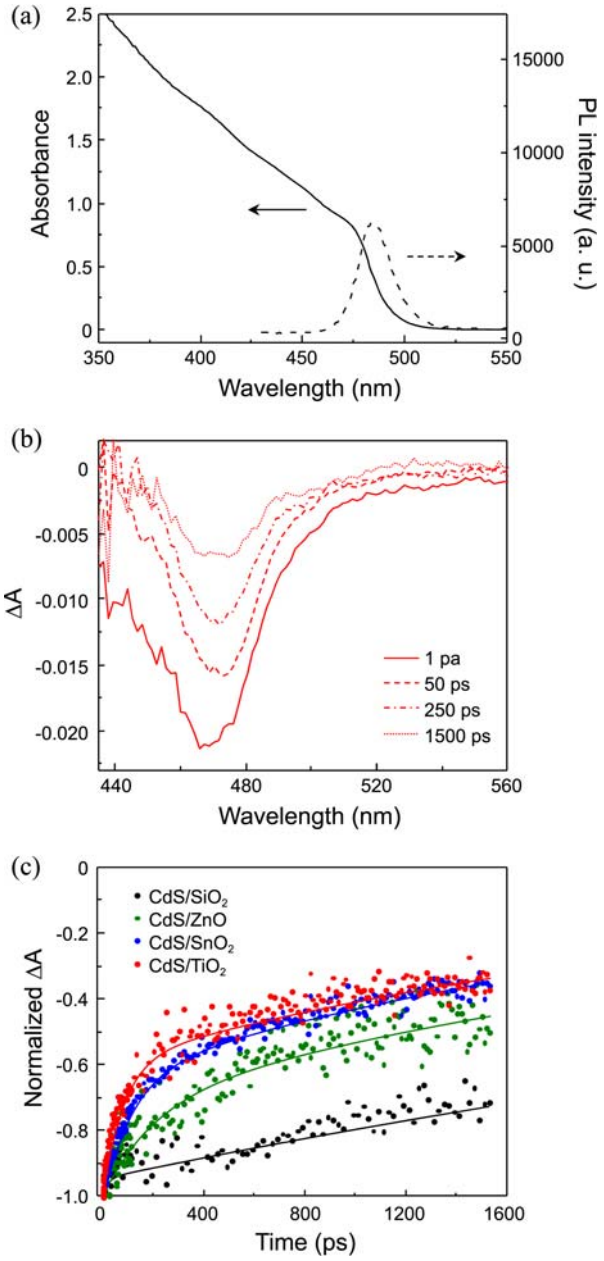

Figure 1. (a) UV-vis absorption and photoluminescence spectra of CdS QDs, (b) transient absorption spectra of CdS QDs anchored on TiO_2, and (c) bleaching recovery of CdS QDs on various oxide substrates.

QDs were attached onto each oxide film using a linker molecule, 3-mercaptopropionic acid, and photo-induced electron transfer process occurred in each photoelectrode was examined by ultrafast pump-probe laser spectroscopy. Figure 1(b) shows typical time-resolved transient absorption spectra obtained with CdS/TiO_2 photoelectrode, in which bleaching recovery proceeded gradually in the 430-560 nm region.[19] Other photoelectrodes also displayed similar spectra (see Figure S2 in Supporting information), and all spectra were compared with CdS/SiO_2 as a reference. Since SiO_2 is an insulator unlike other oxide films explored in this study, the bleaching recovery occurs only through internal recombination of charge carriers, thus being able to serve as a

control. Upon being excited by laser pulses (387 nm), CdS immediately undergoes charge separation (Eq. 1):

$$\mathrm{CdS} + h\nu \rightarrow \mathrm{CdS\ (h + e)} \quad (1)$$

Electrons in the conduction band of CdS relieve their energy *via* either recombination or electron transfer to oxide (Eqs. 2 and 3), and these relaxation processes appeared as bleaching recovery in time-resolved transient absorption spectra.[20]

$$\mathrm{CdS\ (h + e)} \rightarrow \mathrm{CdS} + h\nu' \quad (2)$$

$$\mathrm{CdS\ (h + e) + oxide} \rightarrow \mathrm{CdS\ (h) + oxide\ (e)} \quad (3)$$

It is evident that the relaxation of photo-induced charge carriers proceeded differently in each photoelectrode when the bleaching recovery recorded at absorption maxima was plotted as a function of time (Figure 1(c)). Provided that charge recombination kinetics within CdS is identical regardless of the nature of oxides, one would speculate that different kinetics of electron injection process in each photoelectrode result in the disparity observed in bleaching recovery.[21,22] The recovery of transient bleaching was analyzed using biexponential fits (Eq. 4) and fitting parameters were tabulated in Table 1.

$$y = A_1 e^{-t/\tau 1} + A_2 e^{-t/\tau 2} \quad (4)$$

Faster bleaching recovery was observed with CdS/TiO_2 and CdS/SnO_2 in comparison with CdS/ZnO, and the apparent electron injection rates obtained using Eq. (5) were 2.3×10^8 s^{-1} (CdS/SnO_2), 1.8×10^8 s^{-1} (CdS/TiO_2), and 1.3×10^8 s^{-1} (CdS/ZnO), respectively.

$$k_{et} = \frac{1}{\langle\tau\rangle_{(CdS/TiO_2,\ CdS/SnO_2,\ or\ CdS/ZnO)}} - \frac{1}{\langle\tau\rangle_{(CdS/SiO_2)}} \quad (5)$$

In general, electron injection kinetics can be expressed by the following equation based on the Marcus theory (Eq. 6):[23]

$$k_{et} = \frac{2}{\hbar}\int_0^\infty dE\rho(E)\left|\overline{H}(E)\right|^2 \frac{1}{\sqrt{4\pi\lambda k_B T}}\exp\left[-\frac{(\lambda+\Delta G_0-E)^2}{4\lambda k_B T}\right] \quad (6)$$

where ΔG_0 is the energy difference between conduction band edges at semiconductor interface, ρ(E) is the density of states at energy E from the conduction band edge, and H(E) is the average electronic coupling between initial and final states of electron transfer, and λ is the total reorganization energy. Since the electron transfer kinetics is influenced by various factors, quantitative comparison among different oxide substrates is very complicated and difficult. Nevertheless, this innately complex system was simplified in this work, trying to provide a qualitative picture on the effect of an oxide substrate on electron transfer kinetics in order to obtain better understanding about the connection between electron transfer kinetics and photoelectrochemical performance. Assuming that the average electronic coupling and the total reorganization energy are nearly identical in all oxide films (this simplification has often been adapted for other systems such as dye/oxide and semiconductor/oxide couples and proved to be acceptable),[21,24] one would expect

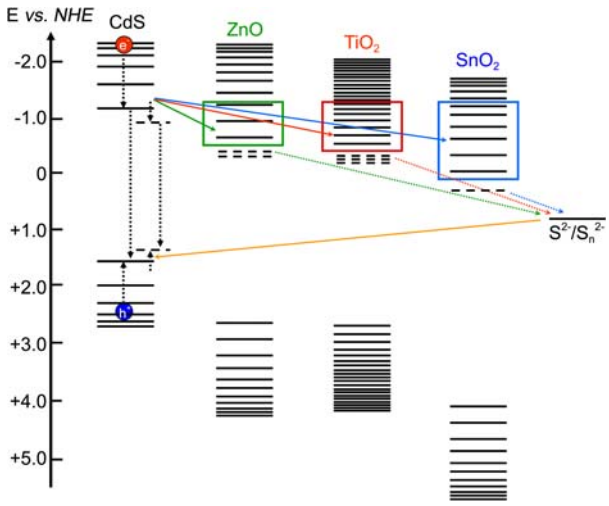

Scheme 1. Energy diagrams of CdS QDs and oxides. Electron transfer process is represented by solid lines and charge recombination by dotted lines, and electron accepting states available are marked with boxes.

that the electron transfer rate is mainly dictated by the free energy difference and the density of states. These two factors differ in each oxide, which is depicted in Scheme 1. Conduction band edges are positioned at 0 V (SnO_2), −0.5 V (TiO_2), and −0.6 V (ZnO), respectively,[16] thus free energy difference is in the order of SnO_2, TiO_2, and ZnO (*i.e.*, ΔG_0 : $SnO_2 >> TiO_2 \approx$ ZnO). On the other hand, the density of states obeys the following relationship (Eq. 7):[23]

$$\rho(E)dE = \frac{(2m^*)^{3/2}}{2\pi^2\hbar^3}\sqrt{E}dE \quad (7)$$

where m^* is the effective mass of electrons in conduction band. The density of states, therefore, is largely dictated by the effective mass of electrons. While there is a controversy about the accuracy of currently known effective mass of electrons for three oxides, it has rationally been accepted that TiO_2 possesses much larger effective mass of electrons in comparison with SnO_2 and ZnO (both have similar values) by an order of magnitude.[25-27] Taking into consideration this discrepancy in the effective mass of electrons, one would consider that TiO_2 has a greater number of acceptor states in conduction band than its counterparts as depicted in Scheme 1 (*i.e.*, $\rho(E)$: $TiO_2 >> SnO_2$ ZnO). Combing these different trends in the free energy difference and the density of states in each oxide derived a conclusion that electron transfer occurred in the CdS/ZnO would be slower than that in other semiconductor couples (CdS/TiO_2 and CdS/SnO_2). This hypothesis was indeed supported experimentally in this study, where faster bleaching recovery was observed in the CdS/TiO_2 and CdS/SnO_2 than in the CdS/ZnO.

Photoelectrochemical Properties. Electron transfer kinetics is intimately related to the performance of photoelectrode. In this study the photoelectrochemical behavior of three electrodes was examined to elucidate the influence of oxide substrates on photoelectrochemical performance. Figure

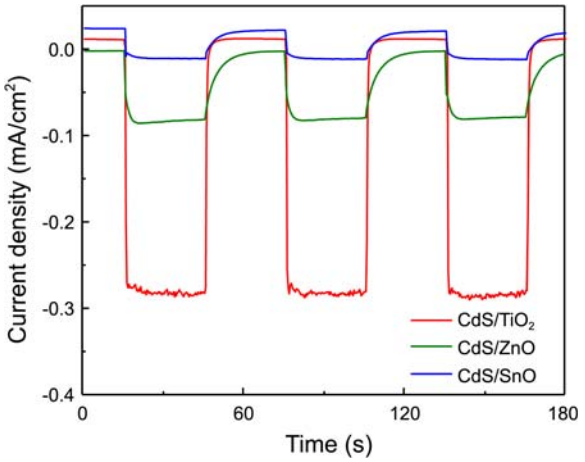

Figure 2. Photocurrent generation in oxide electrodes sensitized with CdS QDs under on/off cycles of illumination ($\lambda > 300$ nm, 100 mW/cm^2).

2 displays photocurrent generation from three photoelectrodes during on/off cycles of light illumination. All photoelectrodes produced photocurrent promptly upon being illuminated, and the photoresponse was steady and reproducible. Of three photoelectrodes, the CdS/TiO_2 photoelectrode was superior to other electrodes in photocurrent generation. The CdS/ZnO photoelectrode was about three-fold less efficient in photocurrent generation than the CdS/TiO_2, and the CdS/SnO_2 photoelectrode barely produced photocurrent. It is important to note that significant dark current (*i.e.*, cathodic current) was observed in the case of the CdS/SnO_2 photoelectrode, which arises from the recombination of electrons with oxidized species of S^{2-} ions (*e.g.*, $S^{-\bullet}$, $S_{n+1}^{-\bullet}$, *etc.*) at the electrode/electrolyte interface.[28-31] Such dark current generation was also noticed with the CdS/TiO_2 photoelectrode, while the magnitude of the dark current in comparison with that of photocurrent was very small unlike the CdS/SnO_2 photoelectrode. This observation highlights that there is no direct correlation between electron transfer kinetics and photoelectrochemical performance, which is consistent with recent studies on CdSe QDs/C_{60} and CdSe QDs/oxides photoelectrodes.[21,32]

Charge Recombination. The photoconversion efficiency is in general governed by two main factors: electron injection and charge recombination at electrode/electrolyte interface.[33,34] The discrepancy in trends between electron transfer kinetics and photoelectrochemical behavior on different oxide electrodes suggests that while electron injection process is one of the key steps in dictating photoconversion efficiency, it is not the limiting step for high photoconversion efficiency. This implies that the influence of an oxide substrate on solar performance appears to be more dominating in charge recombination rather than in electron injection kinetics. In order to obtain more insight into the characteristics of charge recombination on different oxide substrates, charge recombination kinetics was investigated by monitoring photovoltage (*i.e.*, open-circuit voltage) decay upon termination of illumination. Open-circuit voltage (OCV) decay mainly arises

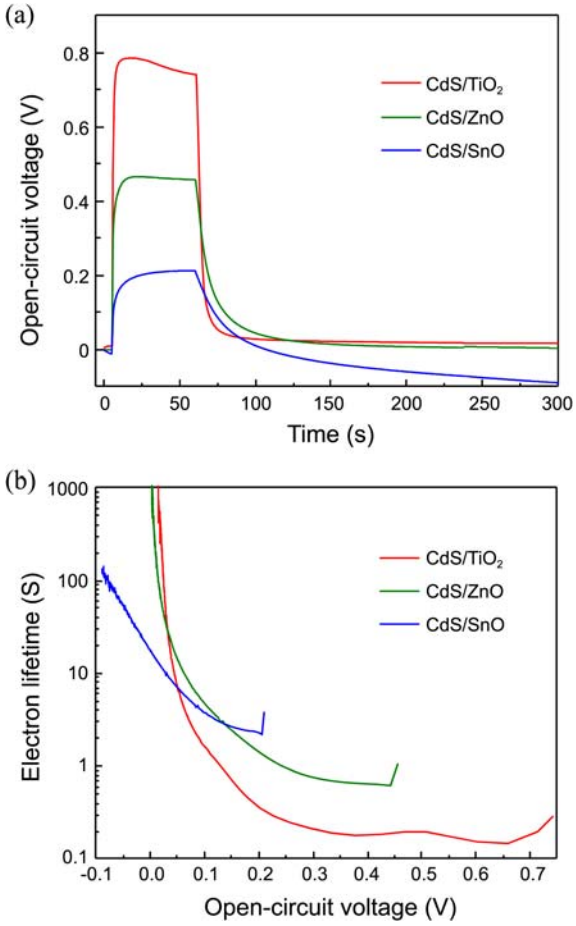

Figure 3. (a) Open-circuit voltage decay and (b) electron lifetime decay of oxide electrodes sensitized with CdS QDs in 0.1 M Na_2S electrolyte.

from charge recombination of injected electrons with oxidized species of redox couple; thus the OCV decay measurement has been widely undertaken as a simple, effective tool to probe charge recombination kinetics. Zaban and co-workers demonstrated that electron lifetime in photoelectrode can be correlated with photovoltage decay rate by the following equation:[35]

$$\tau = \frac{k_B T}{e}\left(\frac{dV_{OC}}{dt}\right)^{-1} \quad (8)$$

where τ is electron lifetime, k_B is Boltzmann's constant, T is temperature, and e is the elementary charge.

Figure 3(a) and (b) show the OCV decay of three photoelectrodes in 0.1 M Na_2S electrolyte and electron lifetime decay obtained using the Eq. (8). The highest OCV was obtained with the CdS/TiO_2 photoelectrode, whereas the lowest OCV with the CdS/SnO_2. Theoretically attainable OCV is mainly determined by conduction band position; therefore, given the conduction band edge position of each oxide (Scheme 1), this observation can be easily rationalized. Despite the favorable conduction band edge position, ZnO yielded a lower OCV than TiO_2. The origin of such low OCV remains elusive and is still under debate at present;[36]

Table 1. Fitted kinetic parameters of bleaching recovery in CdS anchored on oxide substrates. Average lifetimes, $<\tau>$, are determined using the equation, $<\tau> = \Sigma(A_i\tau_i^2)/\Sigma(A_i\tau_i)$

	A_1	τ_1 (ps)	A_2	τ_2 (ps)	$<\tau>$ (ps)
SiO_2	-0.06	20.0	-0.94	5779	5778
ZnO	-0.29	204.6	-0.71	3350	3273
TiO_2	-0.41	85.5	-0.59	2868	2812
SnO_2	-0.37	116.2	-0.63	2547	2484

however, this may be attributed to lower electron injection efficiency from CdS. When analyzing electron injection kinetics, short lifetime component is more important than long lifetime component as it primarily dictates electron injection rate. Comparing the short lifetime component in the CdS/TiO_2 with that of the CdS/ZnO (Table 1), it was much shorter by a factor of ~2.5, indicating that electron injection from CdS to ZnO occured much less efficiently.

On the other hand, OCV decay was much faster in the CdS/TiO_2 electrode than other electrodes, suggesting that the CdS/TiO_2 electrode is the most vulnerable to charge recombination, whereas the CdS/ZnO electrode is least subjected to the loss of electrons. An interesting observation was that the OCV decay converged to –0.2 V, not 0 V, in the case of the CdS/SnO_2 electrode. This observation implies that the substantially high cathodic current (dark current) flowed when SnO_2 was employed as a substrate, which is consistent with the observation in photocurrent measurement. The fast recombination observed with the CdS/SnO_2 results from the location of conduction band of SnO_2, which is lower than TiO_2 by ~0.5 V.[26] While the lowly positioned conduction band is more favorable for electron injection from CdS as confirmed in this study, this can also facilitate charge recombination between the injected electrons and redox couple. As a result, the CdS/SnO_2 electrode showed the worst photoelectrochemical performance among the three electrodes in spite of the fastest electron injection rate. The CdS/TiO_2 electrode also suffered from serious charge recombination; however, no significant dark current was observed in the CdS/TiO_2 electrode unlike the CdS/SnO_2 electrode. While the charge recombination was problematic in the CdS/TiO_2 electrode, its photoelectrochemical performance exceled that of other electrodes. In the case of the CdS/ZnO, the photogenerated electrons accumulated within ZnO were not readily recombined with redox couple; thus CdS/ZnO electrode exhibited longer electron lifetimes. Despite the reduced charge recombination at the electrode/electrolyte interface, the electron injection rate in the CdS/ZnO was slower than other electrodes, giving rise to modest photoelectrochemical performance.

Conclusions

CdS-sensitized oxides were investigated as a model system to probe the effect of oxide substrates on photoelectrochemical performance. This study reveals that the influence of an oxide substrate on electron injection kinetics and charge recombination appears to be intricate and is difficult to be explained with a simple, generalized theory. While more study is still required to establish a general explanation on this fundamental processes dictating solar cell performance, the current study provided a qualitative picture on the relationship between these critical processes and photoelectrochemical behavior. Spectroscopic analysis showed that electron injection kinetics played a role in photoelectrochemical performance to some extent, but its influence on photoelectrochemical performance was limited. Suppressing charge recombination at photoelectrode/electrolyte is another critical factor to be considered when constructing a high performance photoelectrode. The OCV decay analysis combined with photocurrent measurement unveiled that SnO_2 suffered from serious charge recombination, whereas ZnO was more resistive against the interfacial charge recombination. Despite the fast charge recombination rate, TiO_2 showed the best performance among three oxides, suggesting that electron injection kinetics and charge recombination were optimized best in TiO_2 among three oxides examined in this study. This implies that developing a strategy to impede charge recombination at TiO_2/electrolyte interface would be of great importance in order to achieve high performance. This study also suggests that ZnO and SnO_2 may have a chance to overtake TiO_2 in spite of several issues, if a novel strategy could be developed to improve electron injection rate (for ZnO) or suppress charge recombination (for SnO_2).

Acknowledgments. I thank Prof. P. V. Kamat for helpful discussion. The experiments were carried out at Radiation Laboratory, University of Notre Dame, which is supported by the Department of Energy, Office of Basic Energy Sciences. I acknowledge the research fund provided by Hanyang University (HY-2010-N).

Supporting Information Available. SEM and XRD analysis of SnO_2, ZnO, and TiO_2 films; transient absorption spectra of CdS QDs anchored on various metal oxides.

References

1. Hodes, G. *J. Phys. Chem. C* **2008**, *112*, 17778.
2. Kamat, P. V.; Tvrdy, K.; Baker, D. R.; Radich, J. G. *Chem. Rev.* **2010**, *110*, 6664.
3. Hod, I.; González-Pedro, V.; Tachan, Z.; Fabregat-Santiago, F.; Mora-Seró, I.; Bisquert, J.; Zaban, A. *J. Phys. Chem. Lett.* **2011**, *2*, 3032.
4. Yang, Z.; Chen, C.-Y.; Roy, P.; Chang, H.-T. *Chem. Commun.* **2011**, *47*, 9561.
5. Vogel, R.; Hoyer, P.; Weller, H. *J. Phys. Chem.* **1994**, *98*, 3183.
6. Kamat, P. V. *J. Phys. Chem. C* **2008**, *112*, 18737.
7. Bang, J. H.; Kamat, P. V. *ACS Nano* **2009**, *3*, 1467.
8. Ji, I. A.; Park, M.-J.; Jung, J.-Y.; Choi, M. J.; Lee, Y.-W.; Lee, J.-H.; Bang, J. H. *Bull. Korean Chem. Soc.* **2012**, *33*, 2200.
9. Peter, L. *Acc. Chem. Res.* **2009**, *42*, 1839.
10. Mora-Seroì, I.; Bisquert, J. *Nano Lett.* **2003**, *3*, 945.
11. Tiwana, P.; Docampo, P.; Johnston, M. B.; Snaith, H. J.; Herz, L. M. *ACS Nano* **2011**, *5*, 5158.
12. Snaith, H. J.; Ducati, C. *Nano Lett.* **2010**, *10*, 1259.

13. Leschkies, K. S.; Divakar, R.; Basu, J.; Enache-Pommer, E.; Boercker, J. E.; Carter, C. B.; Kortshagen, U. R.; Norris, D. J.; Aydil, E. S. *Nano Lett.* **2007**, *7*, 1793.
14. Hossain, M. A.; Jennings, J. R.; Koh, Z. Y.; Wang, Q. *ACS Nano* **2011**, *5*, 3172.
15. Mora-Seroì, I.; Bisquert, J. *J. Phys. Chem. Lett.* **2010**, *1*, 3046.
16. Fessenden, R. W.; Kamat, P. V. *J. Phys. Chem.* **1995**, *99*, 12902.
17. Katoh, R.; Furube, A.; Yoshihara, T.; Hara, K.; Fujihashi, G.; Takano, S.; Murata, S.; Arakawa, H.; Tachiya, M. *J. Phys. Chem. B* **2004**, *108*, 4818.
18. Nonoguchi, Y.; Nakashima, T.; Kawai, T. *Small* **2009**, *5*, 2403.
19. Zhang, J.; Tang, C.; Bang, J. H. *Electrochem. Commun.* **2010**, *12*, 1124.
20. Robel, I.; Subramanian, V.; Kuno, M.; Kamat, P. V. *J. Am. Chem. Soc.* **2006**, *128*, 2385.
21. Tvrdy, K.; Frantsuzov, P. A.; Kamat, P. V. *Proc. Nat. Acad. Sci. U.S.A.* **2011**, *108*, 29.
22. Dibbell, R. S.; Youker, D. G.; Watson, D. F. *J. Phys. Chem. C* **2009**, *113*, 18643.
23. Asbury, J. B.; Hao, E.; Wang, Y.; Ghosh, H. N.; Lian, T. *J. Phys. Chem. B* **2001**, *105*, 4545.
24. Stockwell, D.; Yang, Y.; Huang, J.; Anfuso, C.; Huang, Z.; Lian, T. *J. Phys. Chem. C* **2010**, *114*, 6560.
25. Bauer, C.; Boschloo, G.; Mukhtar, E.; Hagfeldt, A. *J. Phys. Chem. B* **2001**, *105*, 5585.
26. Green, A. N. M.; Palomares, E.; Haque, S. A.; Kroon, J. M.; Durrant, J. R. *J. Phys. Chem. B* **2005**, *109*, 12525.
27. Quintana, M.; Edvinsson, T.; Hagfeldt, A.; Boschloo, G. *J. Phys. Chem. C* **2006**, *111*, 1035.
28. Bang, J. H.; Kamat, P. V. *Adv. Funct. Mater.* **2010**, *20*, 1970.
29. Liu, D.; Kamat, P. V. *J. Phys. Chem.* **1993**, *97*, 10769.
30. Martinez-Ferrero, E.; Mora-Seroì, I.; Albero, J.; Gimenez, S.; Bisquert, J.; Palomares, E. *Phys. Chem. Chem. Phys.* **2010**, *12*, 2819.
31. Chakrapani, V.; Baker, D.; Kamat, P. V. *J. Am. Chem. Soc.* **2011**, *133*, 9607.
32. Bang, J. H.; Kamat, P. V. *ACS Nano* **2011**, *5*, 9421.
33. Guijarro, N. S.; Shen, Q.; Gimeìnez, S.; Mora-Seroì, I.; Bisquert, J.; Lana-Villarreal, T.; Toyoda, T.; Goìmez, R. *J. Phys. Chem. C* **2010**, *114*, 22352.
34. Mora-Seroì, I.; Gimeìnez, S.; Fabregat-Santiago, F.; Goìmez, R.; Shen, Q.; Toyoda, T.; Bisquert, J. *Acc. Chem. Res.* **2009**, *42*, 1848.
35. Zaban, A.; Greenshtein, M.; Bisquert, J. *ChemPhysChem* **2003**, *4*, 859.
36. Sudhagar, P.; Song, T.; Lee, D. H.; Mora-Seroì, I.; Bisquert, J.; Laudenslager, M.; Sigmund, W. M.; Park, W. I.; Paik, U.; Kang, Y. S. *J. Phys. Chem. Lett.* **2011**, *2*, 1984.